The Astrophysical Journal, 572:310–325, 2002 June 10

THE FAR-ULTRAVIOLET SPECTRUM OF TW HYDRAE. I. OBSERVATIONS OF H_2 FLUORESCENCE[1]

Gregory J. Herczeg and Jeffrey L. Linsky
JILA, University of Colorado; and NIST, Boulder, CO 80309–0440; gregoryh@casa.colorado.edu, jlinsky@jila.colorado.edu

Jeff A. Valenti
Space Telescope Science Institute, 3700 San Martin Drive, Baltimore, MD 21218; valenti@stsci.edu

Christopher M. Johns-Krull
Department of Physics and Astronomy, Rice University, 6100 Main Street, MS-108, Houston, TX 77005; cmj@rice.edu

and

Brian E. Wood
JILA, University of Colorado; and NIST, Boulder, CO 80309–0440; woodb@marmoset.colorado.edu
Received 2001 December 12; accepted 2002 January 18

ABSTRACT

We observed the classical T Tauri star TW Hya with the Space Telescope Imaging Spectrograph on board the *Hubble Space Telescope* (*HST*) using the E140M grating, from 1150 to 1700 Å, with the E230M grating, from 2200 to 2900 Å, and with the *Far Ultraviolet Spectroscopic Explorer* from 900 to 1180 Å. Emission in 146 Lyman-band H_2 lines, representing 19 progressions, dominates the spectral region from 1250 to 1650 Å. The total H_2 emission line flux is 1.94×10^{-12} ergs cm^{-2} s^{-1}, which corresponds to 1.90×10^{-4} $L_\odot$ at TW Hya's distance of 56 pc. A broad stellar Lyα line photoexcites the H_2 from excited rovibrational levels of the ground electronic state to excited electronic states. The C II λ1335 doublet, C III λ1175 multiplet, and C IV λ1550 doublet also electronically excite H_2. The velocity shift of the H_2 lines is consistent with the photospheric radial velocity of TW Hya, and the emission is not spatially extended beyond the 0″.05 resolution of *HST*. The H_2 lines have an intrinsic FWHM of 11.91 ± 0.16 km s^{-1}. One H_2 line is significantly weaker than predicted by this model because of C II wind absorption. We also do not observe any H_2 absorption against the stellar Lyα profile. From these results we conclude that the H_2 emission is more consistent with an origin in a disk rather than in an outflow or circumstellar shell. We also analyze the hot accretion region lines (e.g., C IV, Si IV, O VI) of TW Hya, which are formed at the accretion shock, and discuss some reasons why Si lines appear significantly weaker than other TR region lines.

Subject headings: accretion, accretion disks — circumstellar matter — line: identification — stars: individual (TW Hydrae) — stars: pre–main-sequence — ultraviolet: stars

1. INTRODUCTION

T Tauri stars (TTSs) are young (<10 Myr), roughly solar mass stars that have only recently emerged from their natal molecular clouds to become optically visible (see reviews by Bertout 1989; Feigelson & Montmerle 1999). The presence of disks around classical TTSs (CTTSs) is now well established observationally. Millimeter wave measurements of the dust continuum from the outer disk can be used to estimate the disk mass, assuming a dust-to-gas ratio (see review by Zuckerman 2001). Such estimates typically yield masses of $\sim$0.02 $M_\odot$, consistent with the minimum mass for the solar nebula (e.g., Beckwith et al. 1990). Spectral line observations can be used to study the inner regions of the disk through their kinematic signatures. This has been done successfully for very young embedded sources using the infrared (IR) bands of CO (Carr, Mathieu, & Najita 2001; Thi et al. 2001; Najita et al. 1996; Chandler, Carlstrom, & Scoville 1995), but the results are confusing for the CTTSs that show CO band emission (Thi et al. 2001; Chandler et al. 1995).

Molecular hydrogen is expected to be $\sim 10^4$ times more abundant than other gas tracers such as CO in the disks surrounding young stars. Depending on the density, H_2 can survive at temperatures of up to 4000 K (e.g., Williams et al. 2000) and can self-shield well against UV radiation fields, making it an excellent diagnostic of disks around young stars. Good probes of gas in circumstellar disks are needed to determine the lifetime of gas in these environments where planets likely form. Most studies of disks to date have relied on the IR to millimeter wavelength spectral energy distribution (SED) of these young stars. These studies are mainly sensitive to micron-sized dust and have shown that the typical survival time for this dust is only a few million years (Strom, Edwards, & Skrutskie 1993; Wolk & Walter 1996; Hillenbrand & Meyer 1999; Alves, Lada, & Lada 2000). This does not mean, however, that the disks around these stars disappear on this short timescale. Theories of giant planet formation suggest that after the dust collects into larger particles (and no longer shows up in studies of the SED), the gas is still present in the disk for some time before it accretes onto the planets (e.g., Wuchterl, Guillot, & Lissauer 2000). Indeed, if for most CTTSs the gas disappears from the disk on the same timescale as the dust does, it may be quite difficult to form giant gas planets.

Molecular hydrogen around a CTTS was first detected by 2.12183 μm 1–0 $S(1)$ line emission in the spectrum of T Tau (Beckwith et al. 1978). Brown et al. (1981) discovered ultraviolet emission lines of H_2 in an *IUE* spectrum of T Tau and identified them as fluorescent lines pumped by Lyα, which were previously seen in sunspot spectra. In both cases, it was apparent that the molecular hydrogen emission from T Tau is spatially extended. Subsequently, H_2 has been

[1] Based on observations with the NASA/ESA *Hubble Space Telescope*, obtained at the Space Telescope Science Institute, which is operated by the Association of Universities for Research in Astronomy, Inc., under NASA contract NAS5-26555.

studied often around CTTSs in both the IR and UV. Carr (1990) surveyed young stellar objects in the IR, finding H_2 emission in four CTTSs. The location of this H_2 emission is very important. Recent ground-based images of T Tau show that the IR H_2 emission is quite extended, reaching to 20″ from the star (van Langevelde et al. 1994; see also Herbst et al. 1996; Herbst, Robberto, & Beckwith 1997). The extended IR H_2 emission seen around T Tau and other young embedded sources such as L1448 (Bally, Lada, & Lane 1993) is interpreted as shock-heated emission from the interaction of the stellar/disk wind/jet with the surrounding cloud material (see review by Reipurth & Bally 2001). Thi et al. (2001) used the *Infrared Space Observatory* to detect H_2 emission in the IR from 22 CTTSs, Herbig Ae/Be stars, and debris-disk stars, but with a large aperture extending over 20″ this emission may include both disk emission and spatially extended H_2 emission from outflows. They assumed, based on the strength of on-source versus off-source CO emission, that the bulk of the emission occurred in the circumstellar disks. However, Richter et al. (2001) attempted to detect on-source H_2 emission from five of these sources using a small slit but failed to detect any significant H_2 emission.

Magnetic quadrupole transitions of H_2 in the IR are very weak, and electric dipole transitions within the ground electronic state are forbidden because H_2 has no net dipole moment. In the UV, the large oscillator strengths of the electronic Lyman–band (B–X) transitions lead to strong emission and absorption lines via transitions to and from the excited electronic state. Valenti, Johns-Krull, & Linsky (2000) observed H_2 emission in the UV around 13 of 32 TTSs studied with *IUE*. Valenti et al. (2000) go on to argue that the limited sensitivity of *IUE* may be the only reason that H_2 was not detected in the remaining 19 TTS. Johns-Krull, Valenti, & Linsky (2000) attributed UV pumping to the excitation of H_2, because the observed flux in H_2 lines scales with the total UV flux. The UV H_2 lines of T Tau are spatially extended beyond the disks thought to be in this system and may have substantial contributions from outflows. However, as described below, we do not think that the H_2 lines from TW Hya arise in a molecular outflow.

More recently, Ardila et al. (2002) detected fluorescent H_2 around a sample of CTTSs with the *Hubble Space Telescope* Goddard High Resolution Spectrograph (*HST*/GHRS) and attributed the pumping to the red wing of Lyα. Roberge et al. (2001) and Herczeg et al. (2002) presented observations of circumstellar H_2 absorption against the O VI profiles of the Herbig Ae/Be stars AB Aur and DX Cha, as observed with the *Far Ultraviolet Spectroscopic Explorer* (*FUSE*). Herczeg et al. (2002) identified H_2 emission in *FUSE* observations of TW Hya and V4046 Sgr in two Lyman–band H_2 lines but did not detect significant H_2 absorption against O VI for these two stars.

TW Hya is the most prominent member of the recently named TW Hydrae association (TWA; Kastner et al. 1997; Webb et al. 1999), located at a distance of 56 ± 8 pc (Wichmann et al. 1998), making it the closest known CTTS to the solar system. Webb et al. (1999) estimated that TW Hya is a 0.7 $M_\odot$ star with an age of 10 Myr based on evolutionary tracks of D'Antona & Mazzitelli (1997). Most other members of the TWA are naked T Tauri stars (NTTSs—TTSs that lack close circumstellar disks), which confirms that TW Hya is quite old for a CTTS. TW Hya shows strong Hα emission (Rucinski & Krautter 1983; Webb et al. 1999) produced in the accretion column and an IR excess (Jayawardhana et al. 1999) produced by dust emission from a disk. The mass accretion rate has been measured to be in the range $(5\text{–}100) \times 10^{-10}$ $M_\odot$ yr^{-1} (Muzerolle et al. 2000; Alencar & Batalha 2001). By measuring the width of magnetically sensitive lines, Johns-Krull & Valenti (2001b) estimated that the mean magnetic field of TW Hya is on the order of 3 kG. Recent imaging of TW Hya shows that its disk is viewed very nearly face-on (Weinberger et al. 1999; Krist et al. 2000). D. Potter (2001, private communication) determined the disk inclination angle $i = 10° \pm 5°$ using IR polarimetry, while Alencar & Batalha (2001) estimated for the magnetic field an inclination of $i = 18° \pm 10°$ by analyzing time-series profiles of Hα. The outer radius of the disk extends more than 225 AU (Krist et al. 2000; Trilling et al. 2001; Weinberger et al. 2002) from the star, and its inner truncation radius is about 0.3 AU (Trilling et al. 2001). D'Alessio (2001) found evidence from comparing the observed spectral energy distribution of TW Hya to models of SEDs that grains in the inner 0.5 AU of the disk may have grown in size and settled toward the midplane, while dust and gas in the outer disk are well mixed. The disk mass is roughly $(1.5\text{–}3) \times 10^{-2}$ $M_\odot$ (Wilner et al. 2000; Thi et al. 2001; Trilling et al. 2001). On the basis of submillimeter CO emission and estimates for the disk mass, Thi et al. (2001) and van Zadelhoff et al. (2001) determined that CO is underabundant by a factor of $\sim$500 around TW Hya, with respect to a typical interstellar medium (ISM) H_2/CO ratio of 10^4. There is no molecular cloud associated with TW Hya (Webb et al. 1999) and therefore no opportunity to observe whether or not there is an outflow from H_2 or CO observations. Weintraub, Kastner, & Bary (2000) reported the detection of H_2 emission in the 1–0 $S(1)$ line at 2.12183 μm from TW Hya, attributing this line to formation in the circumstellar disk, in which the H_2 is excited by nonthermal electrons produced by X-ray ionization. TW Hya is a strong X-ray source, with $L_X \sim 4 \times 10^{-4}$ $L_\odot$ as measured with *Chandra* by Kastner et al. (2002). These *Chandra* observations indicated an overabundance of Ne, an underabundance of O and Fe, and solar-like abundances of Si, Mg, and N in the X-ray emission region. From the sharply peaked emission measure distribution and high-electron density based on He-like triplets, Kastner et al. (2002) concluded that the X-ray emission is produced in an accretion shock. Alternatively, Gagné et al. (2002) argued that depopulation of the metastable state of the He-like triplets by UV photoexcitation may lead to mistakenly high electron densities.

Here we use *HST*/STIS (Space Telescope Imaging Spectrograph) and *FUSE* spectra of TW Hya to study its circumstellar environment, focusing on the substantial number of H_2 emission lines seen in the UV. In § 2 we explain the observations and data reduction. In § 3 we identify the emission lines and examine their profiles. In § 4 we show that the Si lines are anomalously weak and propose a depletion of Si in the accretion column as one possible explanation. In § 5, we discuss the H_2 fluorescence, and in § 6 we argue that this emission most likely originates in the circumstellar disk of TW Hya. In Paper II, we model the H_2 line fluxes to assess the physical conditions that give rise to the H_2 fluorescence.

2. OBSERVATIONS AND DATA REDUCTION

We used *HST*/STIS to observe the pre–main-sequence star TW Hya on 2000 May 7. We used the medium resolu-

TABLE 1
UV Observations of TW Hya

Date	Data Set	Grating	Time (s)	Aperture (arcsec)	λ_{min} (Å)	λ_{max} (Å)	Resolution
2000 May 7	O59D01020	E230M	1675	0.2×0.2	2157	2965	30,000
2000 May 8	O59D01030	E140M	2300	0.5×0.5	1140	1735	45,800
2000 June 3	P1860101000	*FUSE*	2031	30×30	900	1188	15,000

tion E140M grating and the $0\farcs5 \times 0\farcs5$ aperture for a 2300 s integration (see Table 1). In this paper we only briefly discuss a contemporaneous E230M spectrum of TW Hya.

We reduced the data using the CALSTIS software package (Lindler 1999) written in IDL, which yields equivalent results to the *HST* archive pipeline. Wavelengths were assigned by the reduction software using calibration lamp spectra obtained during the observations. A canonical wavelength solution is determined from a two-dimensional fit of emission lines in a deep lamp exposure. Then a two-dimensional cross-correlation of the deep exposure with a short lamp exposure obtained during the TW Hya observations provides the offset that must be applied to the canonical wavelength solution. Absolute wavelengths are accurate to $\sim$3 km s^{-1}, and relative wavelengths are accurate to $\sim$1 km s^{-1} (Leitherer et al. 2001). Scattered light was removed from the data using the ECHELLE_SCAT routine available in the CALSTIS package, which is identical to the sc2d algorithm used in the standard *HST* pipeline.

We used the *FUSE* satellite to observe TW Hya on 2000 June 6 with the LWRS ($30'' \times 30''$) aperture for a 2081 s integration (Herczeg et al. 2002). We reduced the data using version 1.8 of the CALFUSE pipeline.[2] *FUSE* consists of four gratings with two channels each. The spectrum was rebinned to one wavelength bin per resolution element to increase the signal-to-noise ratio. In this paper we use spectra from the SiC1A, LiF1A, LiF2B, and LiF2A channels, covering the spectral regions 915–1006, 990–1080, 1095–1185, and 1090–1180 Å, respectively. We calibrate the wavelengths of the LiF1A and LiF2A segments using H_2 lines, and of the SiC2A segment using C III ISM absorption, to obtain an accuracy of $\sim$0.1 Å.

3. EMISSION LINES

3.1. *Line Identification*

We detect in the STIS E140M observation of TW Hya over 200 emission lines in the 1140–1710 Å spectral region, shown in Figures 1 and 2. We use a database of over 19,000 H_2 Lyman–band lines (Abgrall et al. 1993) and the Kurucz & Bell (1995) atomic line database to identify lines based upon both coincidence with calculated (for H_2) or lab rest wavelengths (for atoms) and consistency of fluxes with predicted branching ratios from the upper state for H_2 lines.

We identify 146 H_2 lines, including five blends, from 19 excited levels, listed in Table 2 by upper level. Following conventional spectroscopic notation, these lines are identified as *R* or *P* depending on the change in rotational quantum number of $J' - J'' = -1$ or $+1$, respectively, where J' refers to the rotational quantum number of H_2 in the upper excitation state and J'' refers to the rotational quantum number in the lower excitation state. For example, the line 0–4 *P*(1) at 1335.921 Å is the transition between $v'' = 4$, $J'' = 1$ in the ground electronic state and $v' = 0$, $J' = 0$ in the excited electronic state. We use the term "progression" to indicate the set of *R* and *P* transitions from a single excited level to the various available levels in the ground electronic state, as demonstrated in Figure 3. We describe our identification of lines by analyzing in detail the lines from the $v' = 0$, $J' = 17$ level in the excited electronic state. Table 3 shows the possible radiative transitions from this state. We detect five of the six transitions with the largest radiative de-excitation rates, A_{ul}, and calculate that the flux ratios are consistent with the branching ratios. The only undetected line among the strongest six transitions is 0–5 *P*(18) at 1548.146 Å. The flux at this wavelength is dominated by the blue side of the C IV λ1548 line, making the detection of the H_2 line difficult. In addition to these 146 H_2 lines from our STIS observations, Figure 4 shows the detection of the Lyman–band H_2 transitions 1–1 *P*(5) at 1161.864 Å and 1–1 *R*(3) at 1148.751 Å in the *FUSE* spectra of TW Hya (Herczeg et al. 2002).

In Table 4 we list 15 tentatively identified H_2 Lyman–band lines from 10 different excited levels. Based on branching ratios, these lines should be among the strongest lines from a given excited level, and a transition to that excited level coincides with a strong emission feature. For these tentative identifications, emission in the other transitions from the same upper level is either masked by strong emission features, occurs shortward of the spectral region we observed, is obscured by a wind absorption feature in an atomic line, or is too weak to be clearly identified as emission. For example, we identify a narrow feature at 1593.826 Å tentatively as emission in the H_2 transition 3–10 *R*(5), the second strongest transition from $v' = 3$, $J' = 6$, with a calculated rest wavelength of 1593.751 Å. The strongest transition from this excited state, 3–10 *P*(7) at 1611.315 Å, appears to be weakly present. The third and fourth strongest lines, 3–1 *R*(5) and 3–1 *P*(7), have wavelengths shortward of the STIS bandpass. This observation is too short to detect the weaker lines. The excited level for this transition may be pumped by C III via the 3–2 *R*(5) transition at 1175.248 Å. We do not use these tentatively identified H_2 lines in further analysis.

A similar test of over 75,000 CO lines from the Kurucz database failed to identify any groups of CO lines in the spectrum of TW Hya; we therefore consider the coincidence of individual CO transitions with observed emission lines as random chance. The usual electronic pumping routes through the O I multiplet at 1305 Å, as seen in giant stars such as α Boo (Ayres 1986; Ayres et al. 2001a) do not appear to occur in TW Hya (see Fig. 5). A number of weak, narrow emission lines from 1354 to 1357 Å may be CO A–X emission, pumped by H_2 emission at 1393.9 Å via transitions within the thermal width of the H_2 line.

[2] See the Calfuse Pipeline Reference Guide at http://fuse.pha.jhu.edu/analysis/pipeline_reference.html.

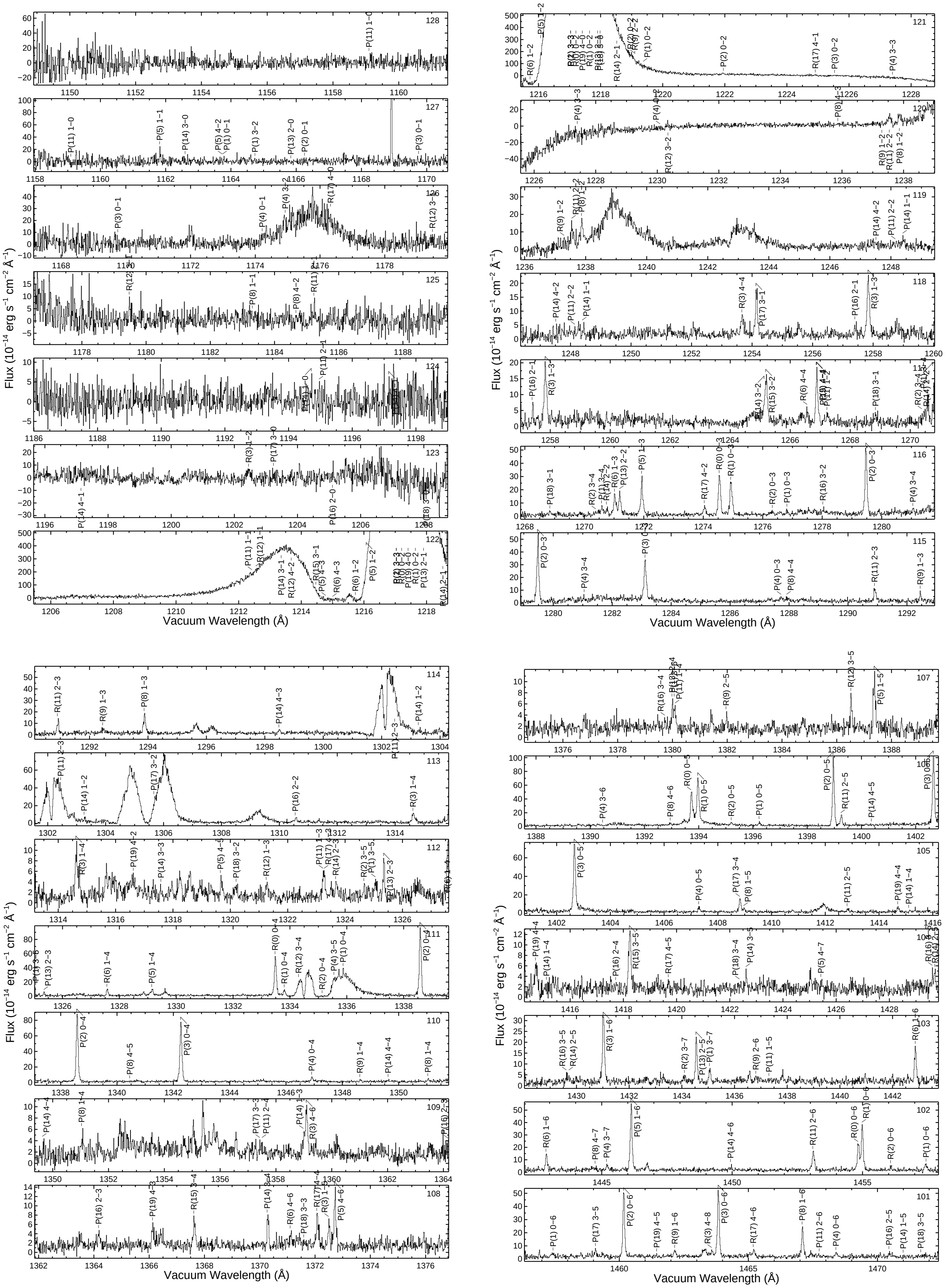

FIG. 1.—*HST*/STIS E140M spectrum of TW Hya. Lyman-band transitions of H_2 that may be pumped by Lyα are labeled. Some of these transitions are too weak to be detected.

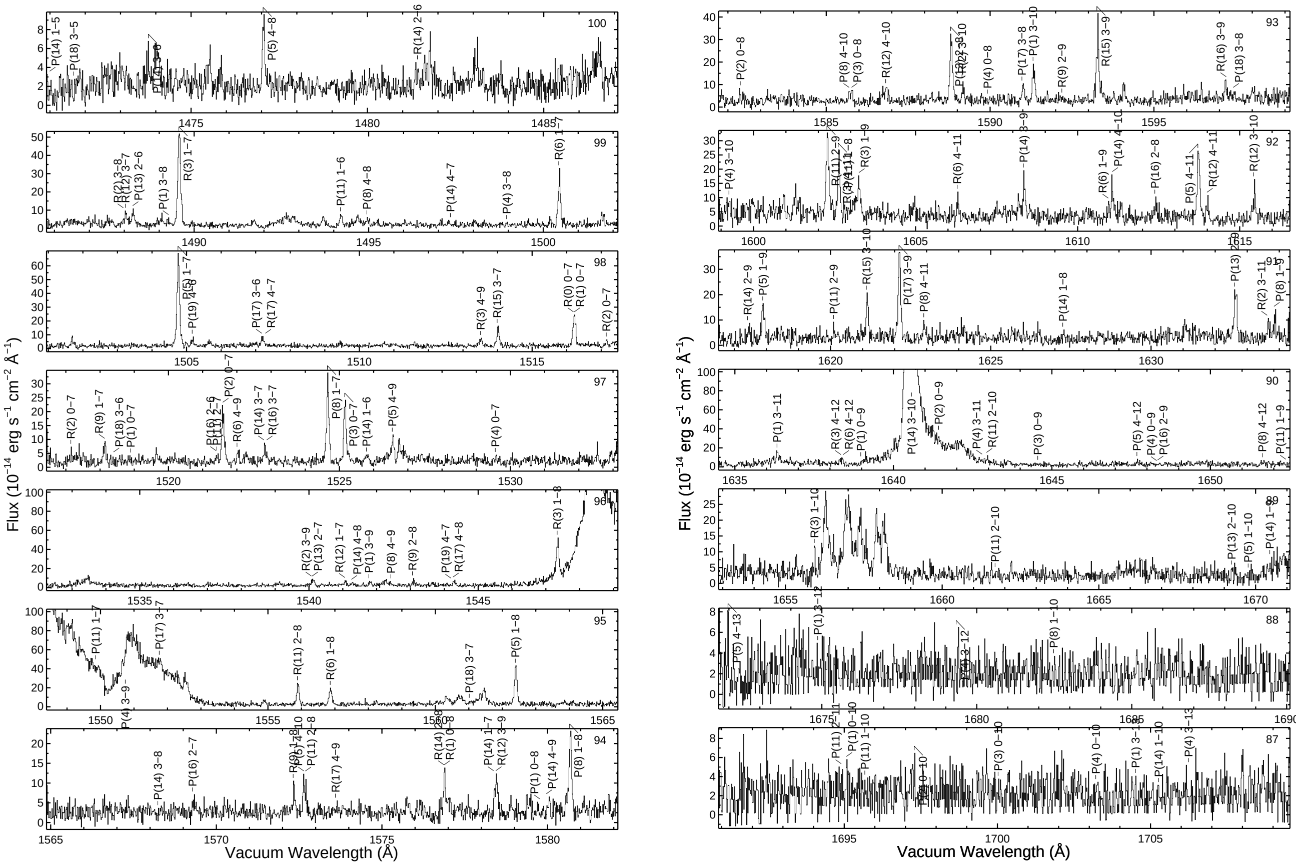

FIG. 1.—*Continued*

3.2. *Spatial Extent of Emission*

Observing with a 0″.5 × 0″.5 aperture, for TW Hya's distance of 56 pc, we detect H_2 emission that occurs spatially within 14 AU of the star. The STIS E140M mode can provide some information on the spatial extent of the H_2 emission across the aperture. We analyze separately the spatial distribution of H_2 lines with wavelengths $\lambda < 1350$ Å, $1350 < \lambda < 1500$ Å, and $\lambda > 1500$ Å, because the width of the instrumental spatial profile increases toward lower wavelengths (Leitherer et al. 2001). In this analysis, we do not use H_2 lines contaminated by N V, C II, Si IV, or C IV emission. We coadd the spatial extent of many H_2 lines and compare their spatial distribution to other lines with similar wavelengths. The Lyα λ1215.67 line, the C IV λ1549 doublet, and the He II λ1640 line are probably produced in the accretion shock near the stellar surface (e.g., Calvet et al. 1996) and therefore should be spatially unresolved and represent a good estimate of the spatial profile in the cross-dispersion direction. Cooler lines, such as the O I λ1304 triplet and the C I multiplets at 1561 and 1657 Å, may be produced in the accretion shock or may also be somewhat extended. The geocoronal Lyα line uniformly fills the aperture.

We use the order locations on the detector to identify the location of each H_2 line and then extract a subimage, a 15 × 15 pixel region around the brightest pixel at this location. We coadd these subimages and then create normalized spatial profiles for H_2 from 3 pixel (0″.11) wide swaths and for atomic lines from 7 pixel (0″.26) wide swaths centered on the brightest pixel. Although the brightest pixel is offset in different wavelength bins by up to half a pixel, this only slightly affects the central region of the spatial profile and does not affect the wings of the profile. Figure 6 shows that the H_2 profile has more power in the wings of the spatial profile than the high-temperature lines and O I, although the wings are comparable to the extent of C I emission. Geocoronal Lyα emission, which uniformly fills the aperture, is clearly more extended than the H_2 emission.

In Figure 6*c* we compare the spatial extent of C IV emission and H_2 emission lines above 1500 Å. We split these H_2 lines into nine lines with flux above and 36 lines below 3×10^{-14} ergs cm^{-2} s^{-1}. The stronger H_2 lines do not show the broad wings that the weak emission lines show. Similarly, we compare C IV emission at the peak wavelength to C IV emission on the edge of its spectral profile. The spatial profile from the peak emission strongly resembles the spatial profile of the strong H_2 lines, while the spatial profile from the weak wings of the C IV profile strongly resembles the spatial profile of the weak H_2 emission lines. This relationship, with weak H_2 lines having broader wings than strong H_2 lines, holds for all wavelengths. This weak emission in the wings may be due to a weak extended background UV source or detector background. We conclude that the H_2 emission is not extended in the cross-dispersion direction beyond the 0″.05 resolution of the telescope, comparable to 2.8 AU, or a 1.4 AU radius from the central star.

3.3. *Line Profiles*

We fitted most of the emission lines with either a single or, for blended lines, multiple Gaussians. Several lines were not fitted because their profiles are non-Gaussian, as shown by

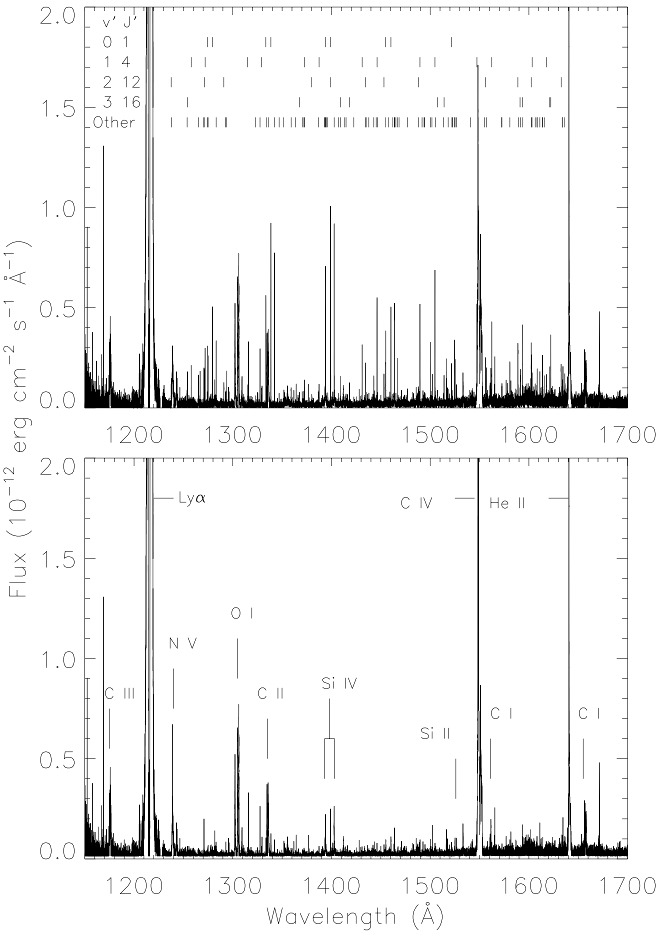

FIG. 2.—E140M spectrum of TW Hya. H_2 lines are marked (*top*) from four upper states, while H_2 lines in all other progressions are marked together. The spectrum without H_2 lines is shown below.

many examples in Figure 7. The profiles of Lyα λ1215.67, the C IV λ1549 doublet, the N V λ1240 doublet, the He II λ1640.5 line, the C III λ977 line, and the C II λ1335.7 line show strong redshifted emission with a sharp blue edge. ISM absorption appears in the O I λ1302, C II λ1334.5 line, Si II λ1526.7, and in the Mg II λ2800 doublet, centered at the rest wavelength of these transitions in the heliocentric frame. The low-temperature O I λ1305 triplet, C II λ1335 doublet, N I λ1492.6, and Si II lines at 1526.7 and 1533.4 Å, along with the Mg II λ2800 doublet in the near-ultraviolet (NUV), have P Cygni profiles that indicate winds of $\sim$230 km s^{-1}. Physical properties that can be inferred from these lines will be determined in a subsequent paper.

We do not observe H_2 absorption within the Lyα profile, even though the H_2 must absorb the Lyα photons to cause the fluorescence (see § 5). In *HST*/STIS observations of Mira B, Wood, Karovska, & Raymond (2002) detect H_2 absorption against Lyα as well as the corresponding fluorescence. Our *FUSE* observations do not show significant H_2 absorption against the O VI profiles. These unseen H_2 lines, with $v'' = 0$, $J'' = 1$–4, have been observed in other pre–main-sequence stars (Roberge et al. 2001; Herczeg et al. 2002). Because there is no H_2 absorption in our line of sight, if the H_2 is in a circumstellar shell or outflow around TW Hya, then the shell or outflow must be clumpy enough such that the H_2 is not in our line of sight to the star. In Paper II we will quantify this conclusion.

TABLE 2

H_2 PROGRESSIONS

λ_{obs}	ID	$F_{obs}(\sigma)$[a] ($\times 10^{-15}$ ergs cm^{-2} s^{-1})
Pumped by 0–2 P(1) 1219.368 Å		
1335.921............	0–4 P(1)	3.4(0.8)
1396.281............	0–5 P(1)	3.3(0.5)
1457.474............	0–6 P(1)	3.7(0.5)
Pumped by 0–2 R(0) 1217.205 Å		
1274.589............	0–3 R(0)	27.4(1.1)
1279.518............	0–3 P(2)	39.2(1.1)
1333.533............	0–4 R(0)	42.8(1.2)
1338.630............	0–4 P(2)	73.1(1.3)
1393.785............	0–5 R(0)	35.3(1.7)
1399.013............	0–5 P(2)	73.8(1.7)
1454.892............	0–6 R(0)	20.8(1.1)
1460.223............	0–6 P(2)	41.6(1.5)
1516.271............	0–7 R(0)	21.2(b)
1521.647............	0–7 P(2)	16.2(1.1)
Pumped by 0–2 R(1) 1217.643 Å		
1221.971............	0–2 P(2)	9.1(2.2)
1274.980............	0–3 R(1)	24.6(1.0)
1283.161............	0–3 P(3)	28.0(1.2)
1333.851............	0–4 R(1)	7.9(0.7)
1342.314............	0–4 P(3)	64.9(1.3)
1394.021............	0–5 R(1)	52.4(1.9)
1402.707............	0–5 P(3)	73.1(1.8)
1455.038............	0–6 R(1)	30.9(1.4)
1463.885............	0–6 P(3)	42.1(1.4)
1516.372............	0–7 R(1)	21.2(b)
1525.215............	0–7 P(3)	17.9(1.0)
Pumped by 0–2 R(2) 1219.089 Å		
1346.970............	0–4 P(4)	3.8(0.5)
1395.255............	0–5 R(2)	2.4(0.4)
1407.350............	0–5 P(4)	3.0(0.5)
1468.454............	0–6 P(4)	3.4(0.6)
Pumped by 0–5 P(18) 1548.146 Å		
1437.868............	0–3 P(18)	1.6(0.5)
1446.791............	0–4 R(16)	4.4(0.5)
1493.748............	0–4 P(18)	4.7(0.7)
1501.748............	0–5 R(16)	3.8(0.6)
1554.948............	0–6 R(16)	4.3(0.8)
Pumped by 1–2 P(5) 1216.070 Å		
1148.701............	1–1 R(3)	4.6(0.9)[b]
1161.875............	1–1 P(5)	10.9(2.0)[b]
1202.449............	1–2 R(3)	11.3(2.2)
1257.883............	1–3 R(3)	18.1(0.9)
1271.979............	1–3 P(5)	20.5(1.0)
1314.690............	1–4 R(3)	12.2(0.7)
1329.184............	1–4 P(5)	7.5(0.7)
1372.550............	1–5 R(3)	3.2(0.4)
1387.422............	1–5 P(5)	7.1(0.6)
1431.072............	1–6 R(3)	29.0(1.2)
1446.178............	1–6 P(5)	44.2(1.5)
1489.625............	1–7 R(3)	48.2(1.7)
1504.812............	1–7 P(5)	57.5(2.3)
1547.398............	1–8 R(3)	35.3(2.7)
1562.457............	1–8 P(5)	37.2(1.7)
1603.164............	1–9 R(3)	11.2(2.2)
1617.952............	1–9 P(5)	11.6(1.9)

TABLE 2—*Continued*

λ_{obs}	ID	$F_{obs}(\sigma)^a$ ($\times 10^{-15}$ ergs cm^{-2} s^{-1})
Pumped by 1–2 *R*(6) 1215.726 Å		
1237.918	1–2 *P*(8)	11.5(1.3)
1271.074	1–3 *R*(6)	14.1(1.0)
1293.927	1–3 *P*(8)	13.0(0.8)
1327.623	1–4 *R*(6)	6.1(0.7)
1351.100	1–4 *P*(8)	2.8(0.4)
1409.024	1–5 *P*(8)	2.2(0.5)
1442.920	1–6 *R*(6)	11.3(0.7)
1467.147	1–6 *P*(8)	17.6(1.1)
1500.511	1–7 *R*(6)	19.7(1.2)
1524.712	1–7 *P*(8)	23.5(1.3)
1556.921	1–8 *R*(6)	17.0(1.1)
1580.743	1–8 *P*(8)	17.5(1.8)
1633.905	1–9 *P*(8)	5.5(1.5)
Pumped by 1–1 *P*(11) 1212.425 Å		
1267.291	1–2 *P*(11)	2.2(0.6)
1292.507	1–3 *R*(9)	4.9(0.5)
1323.303	1–3 *P*(11)	3.8(0.6)
1380.131	1–4 *P*(11)	3.4(b)
1462.201	1–6 *R*(9)	3.8(0.6)
1494.260	1–6 *P*(11)	4.8(0.6)
1518.184	1–7 *R*(9)	5.6(0.9)
1572.402	1–8 *R*(9)	4.5(0.9)
1603.314	1–8 *P*(11)	9.7(2.2)
Pumped by 2–1 *P*(13) 1217.904 Å		
1237.589	2–2 *R*(11)	8.7(1.1)
1271.238	2–2 *P*(13)	13.5(0.9)
1290.961	2–3 *R*(11)	9.1(0.6)
1380.042	2–4 *P*(13)	2.3(0.5)
1399.304	2–5 *R*(11)	12.1(0.9)
1434.598	2–5 *P*(13)	15.6(0.9)
1453.160	2–6 *R*(11)	15.4(0.9)
1488.306	2–6 *P*(13)	6.8(0.8)
1540.174	2–7 *P*(13)	5.2(b)
1555.950	2–8 *R*(11)	20.1(1.2)
1588.867	2–8 *P*(13)	24.1(1.6)
1602.336	2–9 *R*(11)	28.7(2.5)
1632.688	2–9 *P*(13)	17.5(2.0)
Pumped by 2–1 *R*(14) 1218.521 Å		
1257.460	2–1 *P*(16)	2.7(0.5)
1310.622	2–2 *P*(16)	4.1(0.6)
1323.741	2–3 *R*(14)	2.1(0.4)
1470.513	2–5 *P*(16)	1.9(0.5)
1569.340	2–7 *P*(16)	3.1(0.9)
1612.458	2–8 *P*(16)	3.6(0.9)
1617.505	2–9 *R*(14)	4.1(1.3)
Pumped by 3–3 *P*(1) 1217.038 Å		
1270.631	3–4 *P*(1)	3.1(0.5)
1380.131	3–6 *P*(1)	3.4(b)
1435.112	3–7 *P*(1)	4.0(0.5)
1591.385	3–10 *P*(1)	14.4(1.5)
1636.401	3–11 *P*(1)	7.8(1.8)
Pumped by 3–3 *R*(2) 1217.031 Å and 3–2 *P*(4) 1174.923 Å		
1281.099	3–4 *P*(4)	1.9(0.4)
1434.143	3–7 *R*(2)	1.5(0.4)
1445.258	3–7 *P*(4)	3.1(0.5)
1540.174	3–9 *R*(2)	5.2(b)
1589.226	3–10 *R*(2)	4.6(0.9)
1633.710	3–11 *R*(2)	2.9(0.8)

TABLE 2—*Continued*

λ_{obs}	ID	$F_{obs}(\sigma)^a$ ($\times 10^{-15}$ ergs cm^{-2} s^{-1})
Pumped by 3–1 *P*(14) 1213.356 Å		
1370.343	3–4 *P*(14)	4.0(0.5)
1386.577	3–5 *R*(12)	3.4(0.5)
1422.670	3–5 *P*(14)	1.6(0.4)
1488.100	3–7 *R*(12)	6.7(1.0)
1522.875	3–7 *P*(14)	5.1(0.8)
1578.435	3–9 *R*(12)	8.9(b)
1608.409	3–9 *P*(14)	8.5(1.1)
1616.507	3–10 *R*(12)	6.8(1.4)
Pumped by 3–1 *R*(15) 1214.465 Å		
1254.188	3–1 *P*(17)	11.7(0.8)
1265.232	3–2 *R*(15)	13.6(0.9)
1367.681	3–4 *R*(15)	4.3(0.6)
1408.876	3–4 *P*(17)	11.6(0.7)
1418.291	3–5 *R*(15)	10.9(0.7)
1507.250	3–6 *P*(17)	4.4(0.7)
1514.067	3–7 *R*(15)	10.1(0.9)
1591.064	3–8 *P*(17)	6.3(1.2)
1593.339	3–9 *R*(15)	25.7(1.9)
1621.200	3–10 *R*(15)	11.8(1.5)
1622.205	3–9 *P*(17)	29.7(2.3)
Pumped by 3–0 *P*(18) 1217.982 Å		
1268.890	3–1 *P*(18)	1.4(0.4)
1597.239	3–9 *R*(16)	4.3(1.0)
1597.514	3–8 *P*(18)	2.0(0.9)
Pumped by 4–3 *P*(5) 1214.781 Å		
1253.716	4–4 *R*(3)	6.0(0.7)
1266.930	4–4 *P*(5)	12.9(b)
1359.146	4–6 *R*(3)	6.5(0.8)
1372.768	4–6 *P*(5)	7.2(0.7)
1463.641	4–8 *R*(3)	2.3(0.6)
1477.106	4–8 *P*(5)	5.8(0.7)
1513.566	4–9 *R*(3)	4.3(0.7)
1526.622	4–9 *P*(5)	6.1(1.0)
1572.709	4–10 *P*(5)	6.8(1.1)
1602.689	4–11 *R*(3)	17.6(2.0)
1613.784	4–11 *P*(5)	20.4(1.5)
Pumped by 4–3 *R*(6) 1214.995 Å		
1393.003	4–6 *P*(8)	1.2(0.3)
1522.086	4–9 *R*(6)	2.1(0.5)
1606.359	4–11 *R*(6)	4.4(0.9)
Pumped by 4–2 *R*(12) 1213.677 Å		
1349.699	4–4 *P*(14)	0.8(0.2)
1415.400	4–6 *R*(12)	1.5(0.3)
1509.491	4–8 *R*(12)	1.3(2.9)
1541.331	4–8 *P*(14)	2.2(0.8)
1611.132	4–10 *P*(14)	8.6(1.2)
1614.063	4–11 *R*(12)	4.5(1.1)
Pumped by 4–0 *P*(19) 1217.410 Å		
1266.930	4–1 *P*(19)	12.9(b)
1274.085	4–2 *R*(17)	5.0(0.6)
1372.131	4–4 *R*(17)	4.9(0.6)
1414.761	4–4 *P*(19)	4.6(0.6)
1465.261	4–6 *R*(17)	5.2(0.8)
1505.222	4–6 *P*(19)	3.9(0.8)
1544.345	4–8 *R*(17)	3.6(0.8)

[a] "(b)" indicates blend.
[b] Observed with *FUSE*.

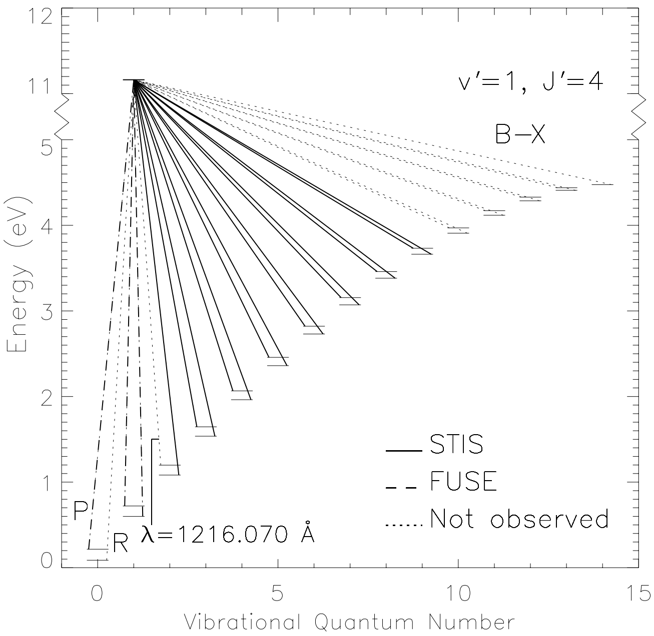

FIG. 3.—H_2 is pumped by Lyα in this example via the 1–2 *P*(5) transition at 1216.070 Å to $v' = 1$, $J' = 4$ at $E' = 11.4$ eV. From this excited electronic level, H_2 returns to many vibrational levels of the ground electronic state via *R* and *P* transitions. We detect emission with STIS (*solid lines*) and *FUSE* (*dashed lines*); no detected emission is indicated by dotted lines.

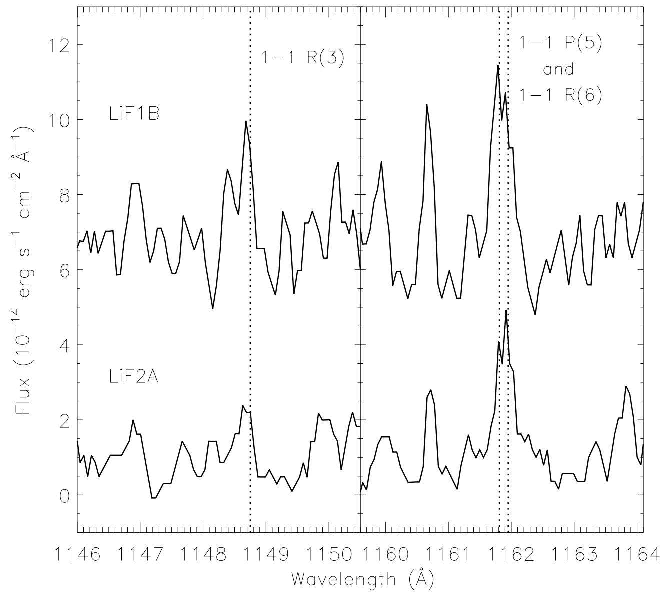

FIG. 4.—*FUSE* observations of two H_2 lines in the LiF1B and LiF2A channels. The flux shown here is smoothed over three resolution elements. The line near 1161.9 Å is a blend of two H_2 transitions, but it is dominated by the 1–1 *P*(5) transition.

The observed Lyα profile is characterized by a strong red wing, possibly produced in the accretion shock, and a dark, wide absorption feature that extends to -700 km s^{-1}. The large width of the Lyα line may be caused by pressure broadening, which Muzerolle, Calvet, & Hartmann (2001) argue produces the broad wings of Hα based on modeling its line profile. The absorption feature is probably caused by a combination of wind, circumstellar, and interstellar absorption. In Paper II we will analyze the Lyα profile in greater detail, including a comparison between the observed Lyα profile and a synthetic Lyα profile reconstructed from H_2 emission line fluxes.

To correct for instrumental line broadening, we now calculate the spectral line-spread function of the detector. We determined in § 3.2 that emission in both atomic and molecular lines is not spatially extended in the cross-dispersion direction. If the emission is also not extended in the dispersion direction, then from the spatial distribution of emission we can determine the spectral line-spread function. We fit multiple Gaussians to the spatial distribution of H_2 in three regions: $\lambda < 1350$, $1350 < \lambda < 1500$, and $\lambda > 1500$. We then multiply the FWHM of these Gaussians by 0.82, which is the ratio of the plate scale of the detector in the cross-dispersion direction to the plate scale in the dispersion direction owing to anamorphic magnification. We then fit emission lines with Gaussians, correcting for the spectral line-spread function, to obtain intrinsic line widths. Parameters of these fits to atomic and unidentified lines are listed in Table 5. We list only the flux from our Gaussian fits to H_2 lines because there are so many, and they are all similar. We measured the flux of the two *FUSE* H_2 in the LiF1B and LiF2A channels separately and coadded the flux of each line, weighted by the error in the flux.

The $0''.5 \times 0''.5$ aperture is not a supported operating mode for STIS. The line-spread function we calculate from the spatial profile of the H_2 emission is similar to the line-spread function determined by Leitherer et al. (2001) for the $0''.2 \times 0''.2$ aperture, and as expected, they are slightly broader for the $0''.5 \times 0''.5$ aperture. We show in Figure 8 that the mean observed FWHM of H_2 lines is 18.16 ± 0.10

TABLE 3
DOWNWARD TRANSITIONS FROM $v' = 0$, $J' = 17$ ARRANGED BY A_{UL}

Wavelength (Å)	A_{ul} (s^{-1})	v''	J''	Flux ($\times 10^{-15}$ ergs s^{-1} cm^{-2})	Wavelength (Å)	A_{ul} (s^{-1})	v''	J''	Flux ($\times 10^{-15}$ ergs s^{-1} cm^{-2})
1501.674........	2.178E+08	5	16	5.01	1604.905........	5.346E+07	7	16	<5
1493.673........	2.107E+08	4	18	4.63	1335.299........	4.231E+07	2	16	<1.5
1446.719........	1.948E+08	4	16	4.35	1647.325........	1.914E+07	7	18	<2.5
1548.146........	1.909E+08	5	18	<20	1325.281........	1.501E+07	1	18	<2.5
1554.849........	1.497E+08	6	16	5.42	1280.162........	9.346E+06	1	16	<2
1437.781........	1.435E+08	3	18	3.03	1650.012........	5.812E+06	8	16	<5
1391.008........	1.132E+08	3	16	<3	1269.897........	1.648E+06	0	18	<2
1599.932........	9.589E+07	6	18	<5	1226.004........	9.338E+05	0	16	<8
1381.413........	6.097E+07	2	18	<3	1687.919........	2.402E+05	8	18	<3

TABLE 4

Tentatively Identified H_2 Lines

λ_{obs}	ID	Flux ($\times 10^{-15}$ ergs cm^{-2} s^{-1})	Pump ID	Pump λ_{calc}	E'' (eV)
1412.887........	2–5 *P*(11)	2.6(0.6)	2–2 *R*(9)	1219.101	1.56
1465.110........	0–6 *R*(5)	2.1(0.6)	0–1 *R*(5)	1173.981[a]	0.72
1363.575........	0–4 *R*(8)	2.3(0.4)	0–3 *P*(10)	1334.497	2.10
1393.506........	0–4 *P*(10)	2.8(1.0)	0–3 *P*(10)	1334.497	2.10
1404.040........	0–4 *P*(11)	2.3(0.5)	0–0 *P*(11)	1175.893	0.88
1522.331........	0–6 *P*(11)	3.7(0.8)	0–0 *P*(11)	1175.893	0.88
1500.244........	0–3 *P*(22)	1.6(0.4)	0–4 *R*(20)	1551.836[b]	3.76
1491.761........	1–7 *P*(2)	3.5(0.6)	1–8 *P*(2)	1550.085[a]	3.36
1498.097........	0–2 *P*(25)	1.4(0.5)	0–3 *P*(25)	1547.971	4.20
1542.322........	0–4 *R*(23)	3.0(0.8)	0–3 *P*(25)	1547.971	4.20
1594.139........	0–4 *P*(25)	2.0(0.9)	0–3 *P*(25)	1547.971	4.20
1359.052........	1–3 *P*(14)	2.6(0.7)	1–1 *R*(12)	1212.543	1.49
1541.125........	1–7 *R*(12)	2.3(0.6)	1–1 *R*(12)	1212.543	1.49
1578.435........	1–7 *P*(14)	8.9[c]	1–1 *R*(12)	1212.543	1.49
1593.826........	3–10 *R*(5)	3.2(0.8)	3–2 *R*(5)	1175.248	1.20
1608.238........	5–12 *R*(6)	2.6(0.8)	5–3 *P*(8)	1218.575	1.89

[a] Unlikely pumping mechanisms.
[b] Also 0–5 *P*(22) at 1550.826 Å.
[c] Flux uncertain due to line blend.

km s^{-1},[3] before removing instrumental broadening. Two lines, 1–8 *P*(11) at 1603.164 Å and 1–4 *R*(3) at 1314.690 Å, have anomalous widths of more than 30 km s^{-1} and are not used in future analysis. After removing instrumental broadening with our calculated spectral line-spread function, the average FWHM of the 30 H_2 lines with fluxes above 2×10^{-14} ergs cm^{-2} s^{-1} is 11.91 ± 0.16 km s^{-1}, which corresponds to a temperature of 6200 K if the broadening were entirely thermal. Although we believe our calculated spectral line-spread function is more accurate for our data than the line-spread function given in Leitherer et al. (2001) for

[3] Errors are 1 σ errors throughout the paper.

TABLE 5

Gaussian-shaped Lines in the E140M Spectrum of TW Hya

ID	λ_{obs} (Å)	v (km s^{-1})	$\sigma(v)$ (km s^{-1})	FWHM (km s^{-1})	σ(FWHM) (km s^{-1})	Flux ($\times 10^{-15}$ ergs cm^{-2} s^{-1} Å^{-1})	$\sigma(F)$ ($\times 10^{-15}$ ergs cm^{-2} s^{-1} Å^{-1})	χ^2
C III...	1175.734	...	...	417	10.3	412	11	1.28
S I......	1295.696	9.7	1.6	47.7	3.70	14.85	0.91	1.05
S I......	1296.231	13.9	2.1	51.4	4.63	11.89	0.83	1.05
Si II....	1309.333	13.1	1.8	133.6	3.90	63.20	1.91	1.55
?........	1315.725	...	1.8	9.6	2.3	2.14	0.37	1.13
C I.....	1328.896	14.4	1.3	10.8	2.71	2.92	0.42	1.19
C I.....	1329.183	18.7	2.1	25.7	2.48	8.33	0.62	1.19
C I.....	1329.652	14.4	1.8	34.5	3.84	8.03	0.79	1.24
Cl I....	1351.709	11.8	3.9	49.5	9.0	4.81	0.66	1.01
?........	1355.434	...	1.9	17.0	1.8	6.17	0.69	0.93
?........	1355.642	...	2.4	14.4	4.8	1.86	0.51	0.93
O I.....	1355.844	54.5	3.0	48.5	7.8	7.53	0.96	0.80
?........	1356.200	...	3.2	15.2	5.4	1.39	0.46	0.80
?........	1360.228	...	7.3	27.8	8.60	2.76	0.66	0.79
Si IV...	1393.935	42.8	2.8	168.3	6.46	75.92	4.51	1.62
Si IV...	1402.828	9.4	3.4	130.2	8.13	34.14	2.74	1.16
S I......	1425.084	11.4	1.7	10.9	3.58	2.07	0.46	1.26
?........	1436.618	...	1.2	12.7	2.92	3.51	0.57	1.02
C I.....	1463.351	3.0	2.2	31.0	4.31	8.99	1.07	0.92
C I.....	1560.403	18.1	1.7	28.6	4.42	12.97	1.64	1.00
C I.....	1560.784	19.6	1.9	48.8	4.42	22.01	2.03	1.00
C I.....	1561.460	23.1	1.6	62.6	3.84	36.79	2.57	1.00
C I.....	1656.362	17.2	1.6	52.5	3.44	53.15	4.17	1.00
C I.....	1657.029	3.8	1.8	49.1	3.98	62.29	4.36	1.28
C I.....	1657.448	12.5	2.9	60.5	7.60	43.67	3.90	1.28
C I.....	1657.967	10.9	1.6	25.3	3.62	27.71	3.05	1.28
C I.....	1658.204	15.0	2.0	36.0	4.88	32.75	3.27	1.28

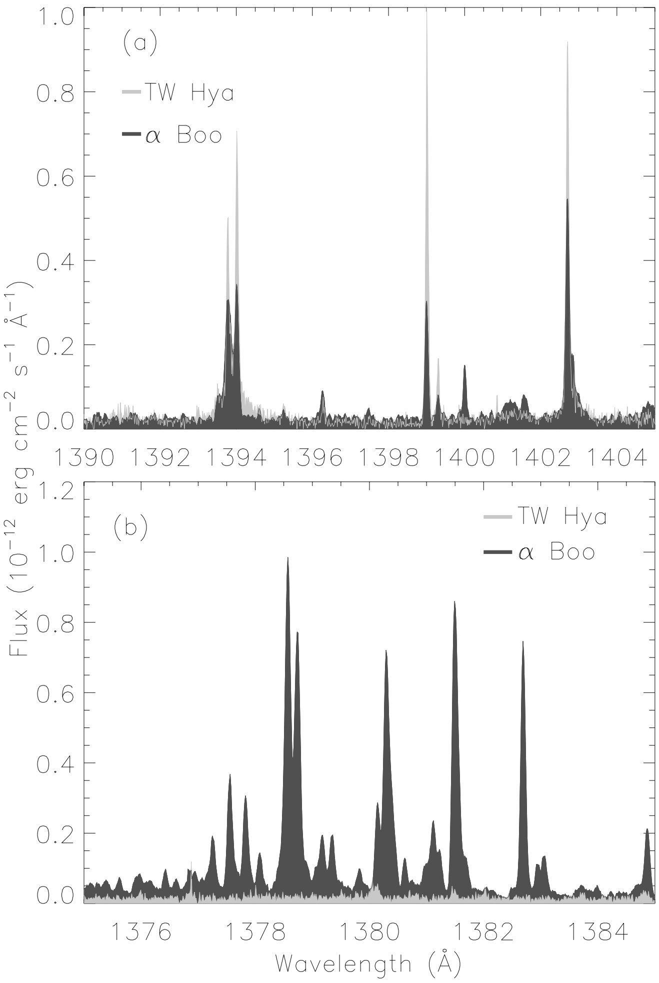

FIG. 5.—Comparison of *HST*/STIS E140M spectra of TW Hya and the evolved giant α Boo (Ayres et al. 2001a). Both stars show narrow H_2 features (*top*) at wavelengths normally dominated by Si IV emission. The spectrum of α Boo has many strong CO A–X lines near 1380 Å, which are pumped by the O I λ1304 triplet, but TW Hya does not show these CO lines.

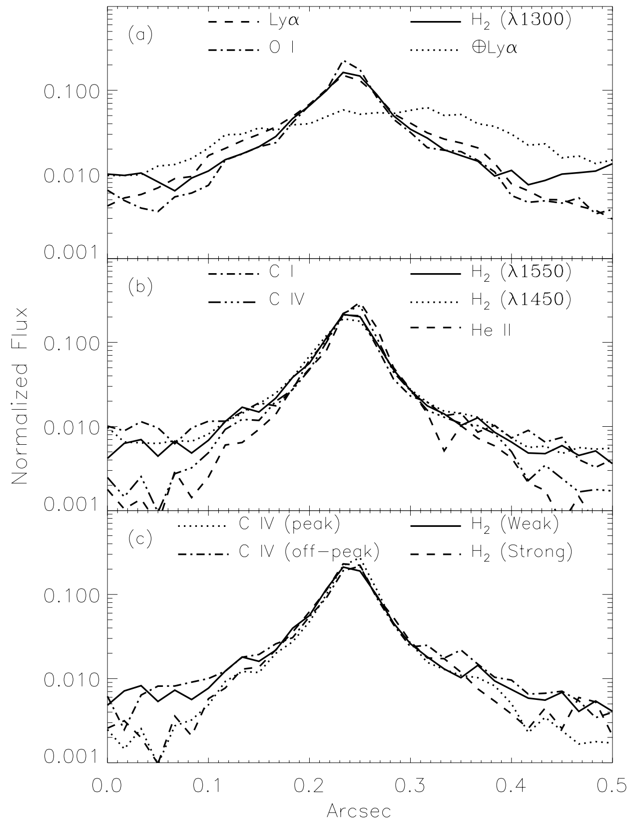

FIG. 6.—(*a*) Spatial extent of H_2 emission (*solid line*) for lines below 1350 Å, compared with Lyα emission (*dashed line*), geocoronal Lyα emission (*dotted line*), and O I emission (*dash-dotted line*) across the aperture in the cross-dispersion direction. (*b*) Spatial extent of H_2 emission (*solid line*) above 1500 Å, compared with H_2 emission from 1350 to 1500 Å (*dotted line*), C IV emission (*triple-dot–dashed line*), He II emission (*dashed line*) and C I emission (*dash-dotted line*), across the aperture in the cross-dispersion direction. (*c*) Spatial extent of strong and weak H_2 lines above 1500 Å compared with C IV emission from its peak and wing.

the $0\farcs2 \times 0\farcs2$ aperture, we calculate an FWHM of 14.2 ± 0.2 km s^{-1} when we correct for instrumental broadening using the line-spread function for the $0\farcs2 \times 0\farcs2$ aperture. In Paper II we will determine the temperature of the H_2 emission region and calculate the nonthermal broadening of the H_2 emission.

Figure 9 shows that the mean velocity shift of 137 H_2 lines is 13.55 ± 0.10 km s^{-1}, with respect to rest wavelengths calculated by Abgrall et al. (1993). We used a conservative error estimate of 0.75 km s^{-1} for the assumed random uncertainty in the rest wavelengths, which is slightly larger than the difference between observed and calculated wavelengths, as given by Abgrall et al. (1993). The velocity shift of H_2 lines, given the approximate ± 3 km s^{-1} uncertainty in wavelength zero-point calibration for STIS E140M spectra (Leitherer et al. 2001), is consistent with previous photospheric radial velocity measurements: 12.2 ± 0.5 km s^{-1} (Weintraub et al. 2000), 12.2 ± 0.1 km s^{-1} (Kastner et al. 1999), 12.5 ± 2.2 km s^{-1} (de la Reza et al. 1989), and 12.9 ± 0.2 km s^{-1} (Torres et al. 1995). The velocity shift for 30 lines shortward of 1350 Å is 13.4 ± 0.2 km s^{-1}, compared with 13.3 ± 0.1 km s^{-1} for 67 lines between 1350 and 1550 Å, and 14.2 ± 0.2 km s^{-1} for 29 lines above 1550 Å, confirming the excellent relative wavelength scale of STIS.

4. HOT ACCRETION LINES

Emission in lines of C IV, Si IV, N V, and O VI, from gas at $\sim 10^5$ K, is probably produced in an accretion flow near the surface of the star (Calvet et al. 1996; Lamzin 1998), as indicated by their broad red wings, which may be produced by rapidly inflowing hot gas. This emission may also be produced in a stellar transition region, although these red wings are broader than emission from most active stars with a coronal emission source (e.g., Ayres et al. 2001b). The ratio of flux in the C IV doublet near 1550 Å to the flux in the Si IV doublet at 1400 Å is 30. In a study of eight CTTSs with *HST*/GHRS, Ardila et al. (2002) found that this ratio varies from 0.5 to 3 in stars that show Si IV emission, but Si IV emission was conspicuously absent from a number of these stars. In spectra of main-sequence and giant stars, the flux ratio of these two doublets is typically about 2 (e.g., Ayres et al. 1997). In giant stars such as α Boo, the Si IV doublet may be absorbed by Si I bound-free absorption below 1525 Å (Ayres et al. 2001a). When this absorption occurs, we expect C I continuum absorption to quench any N V emission, as is observed for α Boo (T. Ayres 2001, private communication), but we detect strong N V emission at 1238 and 1243 Å.

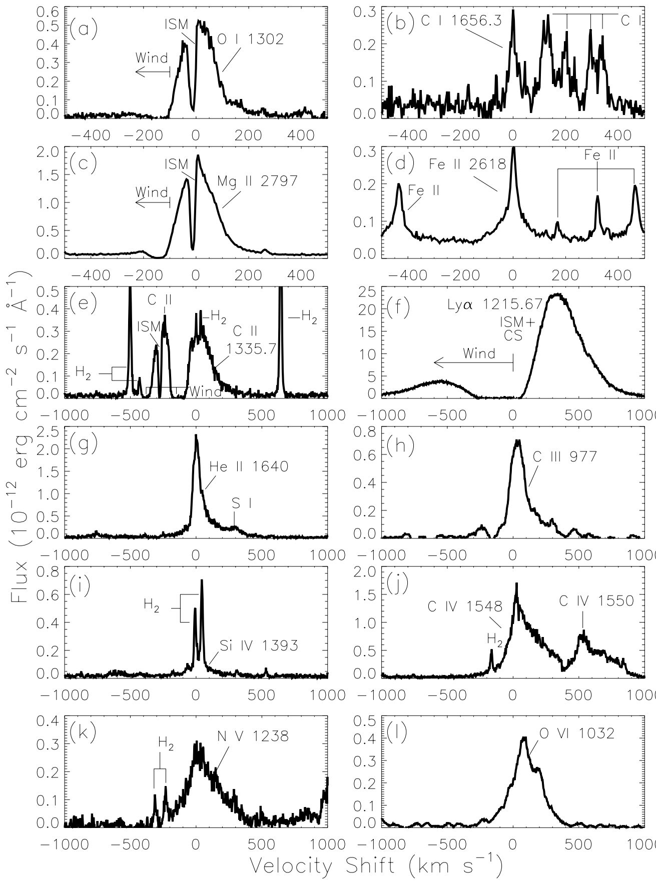

FIG. 7.—Atomic and molecular lines in the STIS and *FUSE* spectra of TW Hya.

Temperature effects probably do not explain the weakness of the Si IV features because it is formed at 80,000 K, close to the 100,000 K formation temperature of C IV. Strong emission in the red wing of the C III line at 977.0 Å indicates the presence of cooler material in the accretion flow, while a strong red wing in C IV, N V, and O VI emission indicates hotter material in the flow.

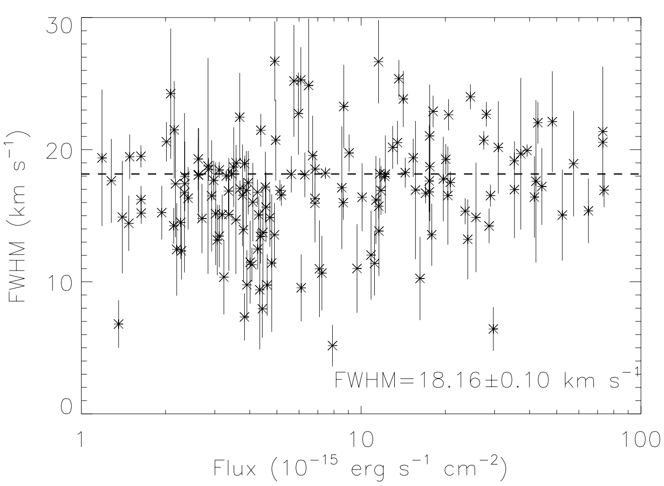

FIG. 8.—FWHM of the H_2 lines, owing to instrumental, thermal, and rotational broadening, plotted here as a function of line flux. The dashed line is the weighted mean of the H_2 FWHM.

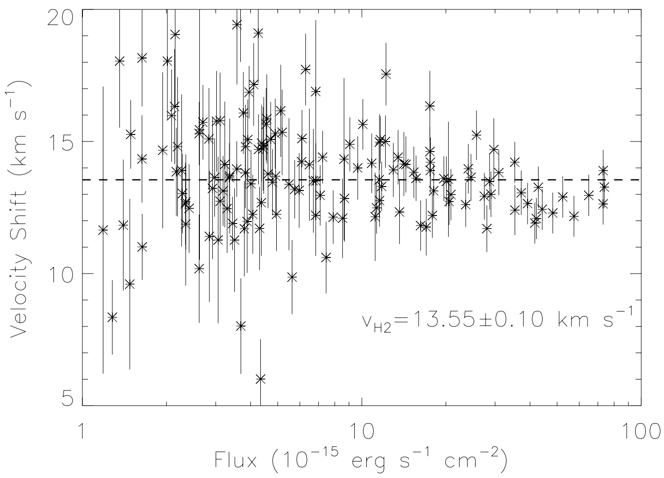

FIG. 9.—Velocity shift of H_2 lines, plotted here as a function of line flux, is consistent with the 12–13 km s^{-1} photospheric radial velocity of TW Hya. The dashed line is the weighted mean of the H_2 radial velocities.

We do not detect Si III features at 1206 and 1296 Å, which are strong in main-sequence and active stars, and the Si II features at 1309.3, 1526.7, and 1533.3 Å are weak. In addition, Valenti et al. (2000) find in *IUE* spectra of TW Hya that the Si III] λ1892 line is also fairly weak, although a reasonable amount of flux is present in the Si II] λ1808 and Si II] λ1817 lines. All of this leads us to speculate that Si may be underabundant in the accretion flow. In the gas phase of the ISM, Si is underabundant by a factor of 100 relative to solar because Si readily depletes onto grains (Fitzpatrick 1996). Chiang et al. (2001) and D'Alessio et al. (1999) provide evidence that grains in a circumstellar disk settle near the midplane. Gammie (1996) showed that ionized material at the surface of the disk couples to the magnetic field, and thereby preferentially accretes onto the star. Silicon may therefore be underabundant in the accretion flow because it is predominantly located in grains at the circumstellar midplane that do not participate in the accretion. If most of the Si is bound in grains, then we might expect strong SiO emission from stellar disks when the accretion shock has underabundant Si IV emission, since the formation of SiO is one step toward the incorporation of Si into dust. Weinberger et al. (2002) and Sitko, Russell, & Lynch (2000) find a broad hump in the IR region 8–13 μm, which they attribute to a combination of silicates, and Weinberger et al. (2002) conclude that the disk of TW Hya contains several hundred Earth masses of condensed silicates and ices. If depletion onto grains in a TTS environment resembles similar processes in the ISM, then other refractory elements such as Fe should also be underabundant. Unfortunately, analysis of the strength of NUV Fe II lines is complicated, partly because most of them are photoexcited by Lyα (Carpenter, Robinson, & Judge 1994; McMurry & Jordan 2000), and there are no other Fe lines available for us to study. Kastner et al. (2002) found solar-like abundances of Si and Mg, an underabundance of Fe and O, and an overabundance of Ne in the *Chandra* spectrum of TW Hya. They attributed the X-ray emission to the accretion shock, which disagrees with previous models in which X-rays from TTSs are produced in a coronae (e.g., Feigelson & Montmerle 1999). If this is the case, then our speculation that Si is underabundant in the accreting gas would be incorrect. We also note that we do not detect Cl I emission at 1351.7 Å, which is strong in most stars owing to pumping by C II. We will pursue these abundance issues further in a future paper.

5. H_2 FLUORESCENCE

We identify 19 progressions of H_2 lines, each with a distinct upper vibrational level v' and rotational level J'. In Table 6, we list these progressions, including the number of detected lines and flux (F_{obs}) in each progression. Ten other progressions listed in Table 3 include the 15 tentatively identified H_2 lines. Figure 10 shows that most levels in the excited electronic state are photoexcited by transitions coincident with Lyα. Figure 11 shows that the lower levels of these transitions are the lowest energy levels with transitions coincident with Lyα, indicating that the level populations

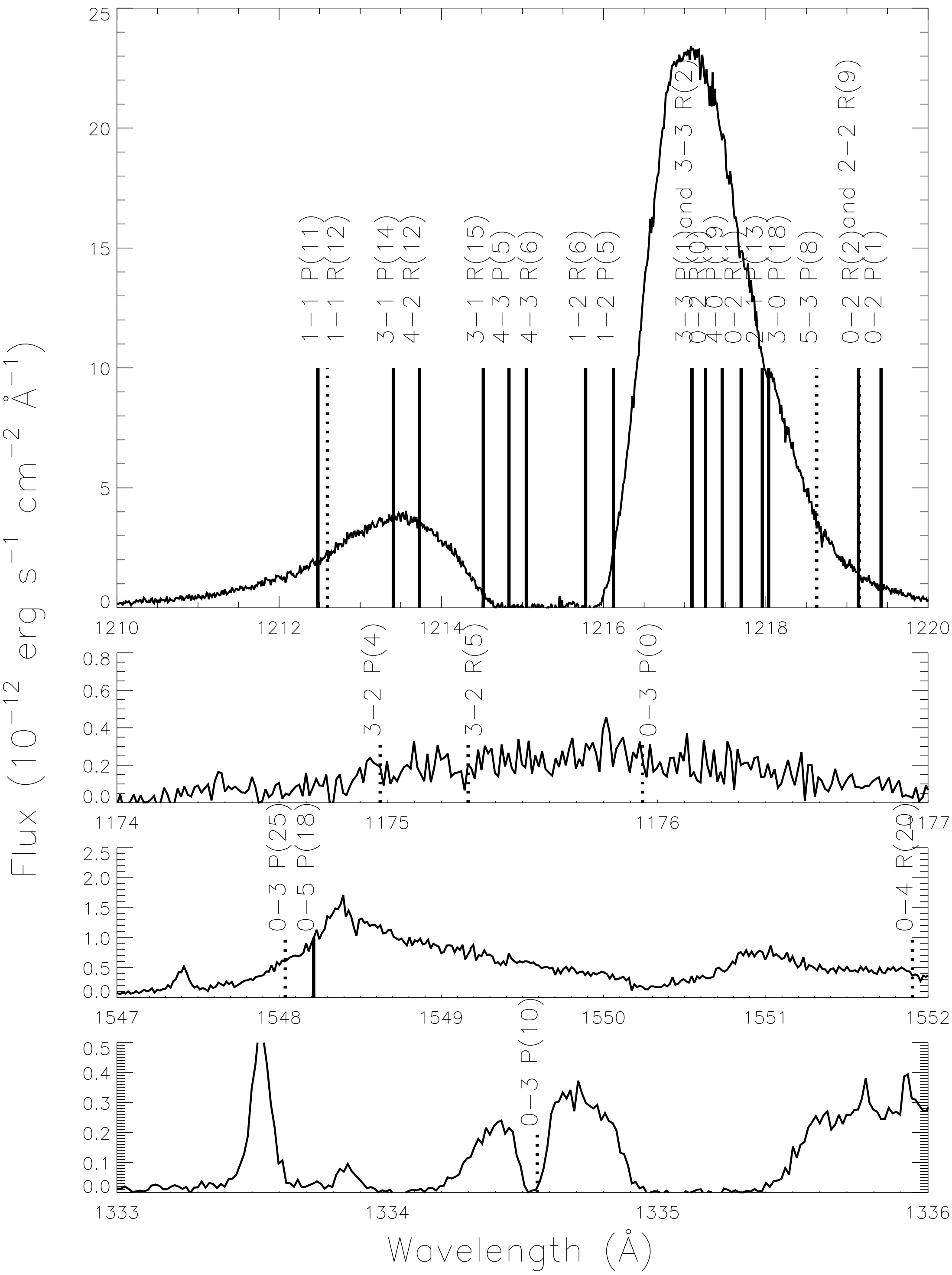

FIG. 10.—H_2 transitions are pumped primarily by Lyα (*top*), although the C III λ1175 multiplet (*second from top*), the C IV λ1549 doublet (*second from bottom*), and the C II λ1334.5 line (*bottom*) also pump some transitions. The solid lines indicate pumping transitions with definite detection of multiple fluorescent lines, and the dotted lines indicate transitions where the fluorescent lines are tentatively detected.

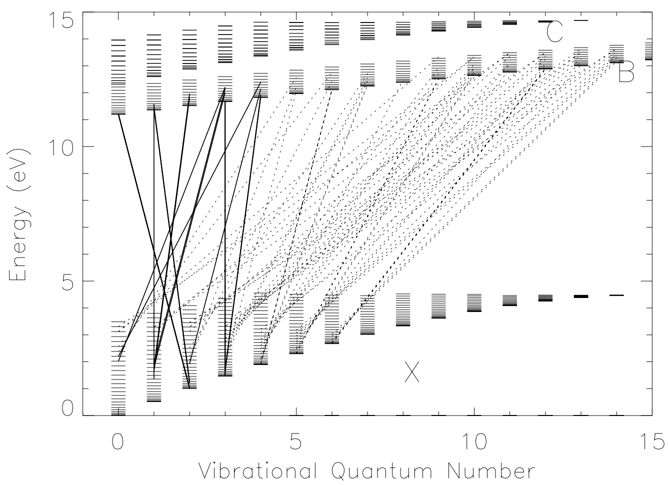

FIG. 11.—Energy levels calculated from transition data in Abgrall et al. (1993) of the ground (X), and excited (B and C) electronic states. Lyman-band (B–X) transitions are discussed in this paper, while Werner band (C–X) transitions typically occur in the *FUSE* bandpass and have no transitions from low-energy levels of the ground state that are coincident with Lyα. We observe fluorescence from upper levels pumped by Lyα via transitions indicated by the solid lines. Dashed lines indicate transitions coincident with Lyα from which fluorescence is not detected. We do not detect fluorescence in progressions pumped from very high energy levels of the ground state, which indicates that the populations of H_2 in the ground electronic state are probably thermal.

may be thermal. The C IV doublet, C II doublet, and C III multiplet also pump some of these levels.

The observed Lyα profile includes a broad absorption feature with FWHM about 500 km s^{-1}, produced by neutral H in the ISM, circumstellar material, and a wind from TW Hya or its disk. We detect no flux owing to either Lyα or H_2 emission in this dark absorption line. This absorption feature coincides with several H_2 transitions that pump the excited state, so most of the Lyα absorption must occur after the Lyα emission encounters the H_2.

We demonstrate the identification of a pumping mechanism for a given excited level by returning to the case of $v' = 0$, $J' = 17$. Because most of the H_2 is in the ground electronic state, and the low-transition probabilities preclude any collisional redistribution of H_2 within the excited electronic state, one of the transitions shown in Table 3 must pump the $v' = 0$, $J' = 17$ level. Of these transitions, only the 0–5 $P(18)$ λ1548.213 line overlaps with a strong emission line observed in the TW Hya spectrum. The weak H_2 feature at 1381 Å is unable to pump a significant amount of H_2 into the $v' = 0$, $J' = 17$ level. The continuum at the wavelengths of these transitions is also unable to pump an appreciable amount of H_2 into this level. The 0–2 $R(16)$ transition, which would be observed at 1335.357 Å, falls in between the C II λ1335 doublet. We do not expect significant blue emission from the 1335.7 Å line in this doublet. The C II λ1334.5 line probably has a strong red wing similar to the C II λ1335.7 line, but this wing is absorbed by a wind in C II λ1335.7. We estimate that the strength of the C II λ1334.5 line at +180 km s^{-1} is $\sim 10^{-13}$ ergs cm^{-2} s^{-1}, which is the strength of the C II λ1335.7 line at the same position. This flux is a factor of 10 weaker than the C IV flux available to pump this upper level. The lower levels for 0–2 $R(16)$ and 0–5 $P(18)$ have energies 2.8 eV and 3.8 eV, respectively, that are too high to have a significant population at sensible temperatures. The $v'' = 5$, $J'' = 18$ level is particularly difficult to populate. We conclude that either the 0–5 $P(18)$ transition at 1548.213 Å or the 0–2 $R(16)$ transition at 1335.357 Å pumps this upper level. The pumping mechanism for almost all other levels is well determined.

The pumping transitions listed in Table 6 require significant populations in the lower rovibrational levels. Changes

TABLE 6

H_2 PUMPING TRANSITIONS

ID	λ_{calc}	v'	J'	v''	J''	E'' (eV)	Number of Lines	F_{obs} (10^{-15} ergs cm^{-2} s^{-1})
3–2 $P(4)$[a]	1174.923	3	3	2	4	1.13	...	...
1–1 $P(11)$........	1212.425	1	10	1	11	1.36	8	39
3–1 $P(14)$........	1213.356	3	13	1	14	1.79	9	42
4–2 $R(12)$	1213.677	4	13	2	12	1.93	6	19
3–1 $R(15)$	1214.465	3	16	1	15	1.94	11	140
4–3 $P(5)$	1214.781	4	4	3	5	1.65	15	96
4–3 $R(6)$	1214.995	4	7	3	6	1.72	3	8
1–2 $R(6)$	1215.726	1	7	2	6	1.27	13	162
1–2 $P(5)$	1216.070	1	4	2	5	1.20	18	350
3–3 $R(2)$	1217.031	3	3	3	2	1.50	5	17
3–3 $P(1)$	1217.038	3	0	3	1	1.48	5	33
0–2 $R(0)$	1217.205	0	1	2	0	1.00	10	395
4–0 $P(19)$........	1217.410	4	18	0	19	2.20	7	36
0–2 $R(1)$	1217.643	0	2	2	1	1.02	11	360
2–1 $P(13)$........	1217.904	2	12	1	13	1.64	13	179
3–0 $P(18)$........	1217.982	3	17	0	18	2.02	3	10
2–1 $R(14)$	1218.521	2	15	1	14	1.79	7	22
0–2 $R(2)$	1219.089	0	3	2	2	1.04	4	13
0–2 $P(1)$	1219.368	0	0	2	1	1.02	3	10
0–5 $P(18)$........	1548.146	0	17	5	18	3.78	5	19

[a] Secondary pump. Primary pump is 3–3 $R(2)$ at 1217.03.

in these level populations may alter which pumping mechanism is most important for certain excited levels. At low temperatures, the ground vibrational level will be much more populated than excited vibrational levels. As a result, $v' = 0$, $J' = 0$ and $v' = 0$, $J' = 3$ would be pumped by the continuum via 0–0 $P(1)$ at 1110.062 Å and 0–0 $P(2)$ at 1110.119 Å, respectively. However, because we do not observe other progressions that would be pumped by the continuum, we conclude that the gas temperature is sufficiently high that Lyα pumps these excited levels. The $v' = 3$, $J' = 3$ level is pumped by both C III 1174 Å via the 3–2 $P(4)$ transition at 1174.923 Å and by Lyα via the 3–3 $P(2)$ transition at 1217.031 Å. Pumping of the $v' = 0$, $J' = 17$ and the tentative route $v' = 0$, $J' = 24$ cannot possibly occur if the H_2 populations are thermal because the energy of the lower level for the routes that populate these levels are very high; we claim that the C IV emission pumps these former via 0–3 $P(25)$ at 1547.971 Å, and that C IV and C II emission pumps the latter, as described above. The lower level $v'' = 3$, $J'' = 25$ for the first transition has an energy of 4.2 eV, compared with the 4.5 eV dissociation energy of the H_2 molecule.

One H_2 transition, 0–4 $R(1)$ at 1333.851 Å, with a flux of $(7.9 \pm 0.7) \times 10^{-15}$ ergs cm^{-2} s^{-1}, is about 6 times weaker than would be expected by branching ratios. Its counterpart, 0–4 $P(3)$ at 1342.314 Å, has a similar branching ratio and lower energy level, and a flux of $(64.9 \pm 1.3) \times 10^{-15}$ ergs cm^{-2}. In Paper II, we will show quantitatively that this particular line is anomalously weak and that it is the only line that is significantly weaker than predicted by our modeling. We conclude that this H_2 line, which is centered at 130 km s^{-1} to the blue side of the C II λ1334.5 line, is absorbed by a wind component of this C II line. This result places the wind in our line of sight to the H_2 emission region and constrains the plausible geometries of TW Hya's circumstellar environment.

We now analyze the velocity shifts and line FWHMs pumped from levels with $E'' < 1.25$ eV and $E'' > 1.5$ eV separately. As discussed in § 3.3, the velocity shift of H_2 lines increases slightly with increasing wavelength, probably because of the relative wavelength accuracy of STIS. We correct for these changes by fitting a line to the velocity shift and wavelength of each transition. We find that the velocity shift of 37 lines pumped from high-energy levels is an average of 0.70 ± 0.16 km s^{-1} above the estimated velocity, while the velocity shift of the 65 lines pumped from low-excitation levels is -0.94 ± 0.15 km s^{-1} from the estimated velocity shift. The accuracy of the wavelengths calculated by Abgrall et al. (1993) compared with laboratory wavelengths indicates that there is most likely not a wavelength bias for high-energy lines. Thus, the difference in the mean velocity shift between the two groups of H_2 lines is likely real.

6. ORIGIN OF H_2 EMISSION

We now consider a circumstellar shell, an outflow, the stellar photosphere, and a disk as possible places of origin for the H_2 emission. We have a number of pieces of evidence to discriminate between models. The H_2 emission is not shifted by more than 3 km s^{-1} relative to the photospheric radial velocity. The spatial extent of the emission indicates that most of it occurs within 0$''$.05 from the star. The Lyα profile shows no H_2 absorption, which gives an upper limit to the amount of H_2 in our line of sight. Finally, the C II wind feature absorbs H_2 emission, which indicates that C II lies in our line of sight to the warm H_2.

Warm molecular emission has in the past been interpreted as shock-heated emission owing to an outflow interacting with the surrounding ambient molecular material. However, the TWA is isolated from any molecular cloud, so this type of emission is difficult to accept. Molecular emission is absorbed by a wind component in the C II line at 1334.5 Å, which would not occur in most shell models. The H_2 progressions pumped near line center of Lyα probably would not occur because of H I absorption in the wind. Assuming the outflow interacts with surrounding material at a large distance from the star, the H_2 emission should be more extended. Consequently, we rule out emission from a surrounding molecular cloud.

Molecular gas could become entrained in an outflow or perhaps form part of the outflow, which could produce emission from hot H_2 gas. In this scenario, the star would have to be extremely close to face-on so that we do not observe either spatial extent in the H_2 emission or H_2 absorption against the Lyα emission. However, we rule out velocity shifts greater than 3 km s^{-1} for the H_2 emission, which is inconsistent with expected outflow velocities.

Johns-Krull & Valenti (2001a) determined that CO absorption near 1.6 μm occurs in the photosphere of most TTSs. The data analyzed here are roughly consistent with an origin of the H_2 emission in the photosphere. If the H_2 is produced in the photosphere, then it should be detected in the IR around NTTSs as well as CTTSs, but this emission has not yet been detected. In a study of H_2 fluorescence with *HST*/GHRS, Ardila et al. (2002) detected H_2 emission from eight CTTSs but did not detect H_2 emission from the one NTTS in their sample. This result is consistent with a disk origin of H_2 emission if the gas disappears from the disk on the same timescales that dust disappears. However, because this H_2 emission is reprocessed Lyα emission, NTTSs may not show H_2 emission because their atomic emission lines are typically weak. Even with weak profiles, Lyα may still be strong near the center of the line profile. In Figure 10, two progressions are pumped near the rest wavelength of Lyα, and fluorescence in these progressions could in principle be seen from NTTSs. This comparison requires further observations with greater sensitivity than *HST*/GHRS offered in order to interpret the results.

We conclude that the most likely site of H_2 emission is in the disk. A disk origin satisfies all of our requirements listed above. The fluorescence could only occur in the surface layer of the disk, because grains would absorb any UV radiation below a certain depth. In Paper II, we will calculate the physical properties of the H_2 emission region. The H_2 fluorescence typically occurs in warm regions ($T \sim 2000$–3500 K), which may pose certain problems in comparing this conclusion with disk models (e.g., D'Alessio, Calvet, & Hartmann 2001; Chiang et al. 2001; Glassgold & Najita 2001). From the temperature of the disk, we will calculate the thermal broadening of the H_2 emission and subsequently spatially constrain the H_2 emission using its orbital velocity.

If this H_2 fluorescence occurs in a disk, then the line profiles from stars with higher inclinations should be wider. In *HST*/STIS spectra of the DF Tau, with an edge-on disk, Linsky, Valenti, & Johns-Krull (1999) found that the FWHM of the H_2 emission lines were typically about 25 km s^{-1}, while we calculate an FWHM of 18 km s^{-1} for the face-on system TW Hya. Johns-Krull & Valenti (2001a) determined from CO absorption that the $v \sin i$ of DF Tau is 18.5 ± 4 km s^{-1}, compared with less than 6 km s^{-1} for TW Hya. The additional broadening observed in the H_2 lines of DF Tau may result from either a faster orbital velocity if the H_2 is in the disk or a faster stellar rotation if the H_2 is in the photosphere.

7. SUMMARY

Our analysis of the ultraviolet spectra of TW Hya obtained with the STIS instrument on *HST* and with *FUSE* lead to the following conclusions:

1. The 1250–1650 Å spectrum is dominated by molecular hydrogen fluorescence in 146 Lyman–band lines. The observed flux in these lines is 1.94×10^{-12} ergs cm^{-2} s^{-1}, corresponding to 1.90×10^{-4} $L_\odot$ at the stellar distance of 56 pc. The H_2 spectrum is pumped to the excited electronic state mainly by transitions coincident with the broad Lyα emission line. Other lines, such as the C II λ1335 doublet, C III λ1175 multiplet, and the C IV λ1550 doublet may also pump some H_2 to the excited electronic state.

2. The H_2 emission is not spatially extended from the star, given a resolution of 0\".05, corresponding to 2.8 AU at 56 pc. With a face-on disk, the H_2 emission is produced within 1.5 AU of the central star.

3. The wavelengths of the H_2 emission is not shifted by more than 3 km s^{-1} with respect to the photospheric velocity of the star.

4. The stellar wind occurs in our line of sight to the H_2 emission region, based upon the anomalously weak flux in an H_2 line that has a wavelength coincident with a wind feature of C II λ1334.5.

5. No significant H_2 absorption is detected against the Lyα profile or the O VI emission lines.

6. The H_2 emission likely originates in the surface layer of a disk, rather than a circumstellar shell or an outflow. We cannot rule out the possibility that the H_2 emission is produced in the stellar photosphere.

7. S II, III, and IV lines are anomalously weak in the UV, possibly because Si depletes onto grains that accumulate in the disk midplane and decouples from the surface material of the disk that preferentially accretes. Thus, the accretion column responsible for the high-temperature emission lines would then be very silicon-poor. Models of the accretion shock are needed to further probe this possibility.

This research is supported by NASA grant S-56500-D to the University of Colorado and NIST, and by a grant to the University of Colorado through the Johns Hopkins University. We thank Tom Ayres, Phil Maloney, David Hollenbach, and Bruce Draine for valuable discussions.

REFERENCES

Abgrall, H., Roueff, E., Launay, F., Roncin, J. Y., & Subtil, J. L. 1993, A&AS, 101, 273
Alencar, S. H. P., & Batalha, C. 2001, ApJ, submitted
Alves, J., Lada, C., & Lada, E. 2000, Ap&SS, 272, 213
Ardila, D. R., Basri, G., Walter, F. M., Valenti, J. A., & Johns-Krull, C. M. 2002, ApJ, 566, 1100
Ayres, T. R. 1986, ApJ, 308, 246
Ayres, T. R., Brown, A., Harper, G. M., Bennett, P. D., Linsky, J. L., Carpenter, K. G., & Robinson, R. D. 1997a, ApJ, 491, 876
———. 2001a, in ASP Conf. Ser. 223, Cool Stars, Stellar Systems, and the Sun, ed. R. Garcia López, R. Rebolo, & M. Zapatero (San Francisco: ASP), 1079
Ayres, T. R., Brown, A., Osten, R. A., Huenemoerder, D. P., Drake, J. J., Brickhouse, N. S., & Linsky, J. L. 2001b, ApJ, 549, 554
Bally, J., Lada, E. A., & Lane, A. D. 1993, ApJ, 418, 322
Beckwith, S. V. W., Gatley, I., Matthews, K., & Neugebauer, G. 1978, ApJ, 223, L41
Beckwith, S. V. W., Sargent, A. I., Chini, R., & Güsten, R. 1990, AJ, 99, 924
Bertout, C. 1989, ARA&A, 27, 351
Brown, A. Jordan, C., Millar, T. J., Gondhalekar, P., & Wilson, R. 1981, Nature, 290, 34
Calvet, N., Hartmann, L., Hewett, R., Valenti, J., Basri, G., & Walter, F. 1996, in ASP Conf. Ser. 109, Cool Stars, Stellar Systems, and the Sun, R. ed. R. Pallavicini & A. K. Dupree (San Francisco: ASP), 419
Carpenter, K., Robinson, R., & Judge, P. 1994, BAAS, 185, 4509
Carr, J. S. 1990, AJ, 100, 1244
Carr, J. S. Mathieu, R. D., & Najita, J. R. 2001, ApJ, 551, 454
Chandler, C. J., Carlstrom, J. E., & Scoville, N. Z. 1995, ApJ, 446, 793
Chiang, E. I. Joung, M. K., Creech-Eakman, M. J. Qi, C., Kessler, J. E., Blake, G. A., & van Dishoeck, E. F. 2001, ApJ, 547, 1077
D'Alessio, P. 2001, in ASP Conf. Ser. 244, Young Stars Near Earth: Progress and Prospects, ed. R. Jayawardhana & T. Greene (San Francisco: ASP), 239
D'Alessio, P., Calvet, N., & Hartmann, L. 2001, ApJ, 553, 321
D'Alessio, P., Calvet, N., Hartmann, L., Lizano, S., & Canto, J. 1999, ApJ, 527, 893
D'Antona, F., & Mazzitelli, I. 1997, Mem. Soc. Astron. Italiana, 68, 4
de la Reza, R., Torres, C. A. O., Quast, G., Castilho, B. V., & Vieira, G. L. 1989, ApJ, 343, L61
Feigelson, E. D., & Montmerle, T. 1999, ARA&A, 37, 363
Fitzpatrick, E. L. 1996, ApJ, 473, L55
Gagné, M., Cohen, D., Owocki, S., & Ud-Doula, A. 2002, ASP Conf. Ser. 262, The High Energy Universe at Sharp Focus, ed. E. M. Schlegel & S. B. Vrtilek (San Francisco: ASP)
Gammie, C. F. 1996, ApJ, 457, 355
Glassgold, A., & Najita, J. 2001, in ASP Conf. Ser. 244, Young Stars Near Earth: Progress and Prospects, ed. R. Jayawardhana & T. Greene (San Francisco: ASP), 251
Herbst, T. M., Beckwith, S. V. W., Glindemann, A., Tacconi-Garman, L. E., Kroker, H., & Krabbe, A. 1996, AJ, 111, 2403
Herbst, T. M., Robberto, M., & Beckwith, S. V. W. 1997, AJ, 114, 744
Herczeg, G. J., Linsky, J. L., Brown, A., Harper, G. M., & Wilkinson, E. 2002, in ASP Conf. Ser., Cool Stars, Stellar Systems, and the Sun (San Francisco: ASP), in press
Hillenbrand, L., & Meyer, M. 1999, BAAS, 195, 0209
Jayawardhana, R., Hartmann, L., Fazio, G., Fisher, R. S., Telesco, C. M., & Piña, R. K. 1999, ApJ, 521, L129
Johns-Krull, C. M., & Valenti, J. A. 2001a, ApJ, 561, 1060
———. 2001b, in ASP Conf. Ser. 244, Young Stars Near Earth: Progress and Prospects, ed. R. Jayawardhana & T. Greene (San Francisco: ASP), 147
Johns-Krull, C. M., Valenti, J. A., & Linsky, J. L. 2000, ApJ, 539, 815
Kastner, J. H. Huenemoerder, D. P., Schulz, N. S., Canizares, C. R., & Weintraub, D. A. 2002, ApJ, 567, 434
Kastner, J. H., Huenemoerder, D. P., Schulz, N. S., & Weintraub, D. A. 1999, ApJ, 525, 837
Kastner, J. H., Zuckerman, B., Weintraub, D. A., & Forveille, T. 1997, Science, 277, 67
Krist, J. E., Stapelfeldt, K. R., Ménard, F., Padgett, D. L., & Burrows, C. J. 2000, ApJ, 538, 793
Kurucz, R. L., & Bell, B. 1995, Kurucz CD-ROM 23, Atomic Line Data (Cambridge: SAO)
Lamzin, S. A. 1998, Astron. Rep., 42, 322
Leitherer, C., et al. 2001, STIS Instrument Handbook (v5.1; Baltimore: STScI)
Lindler, D. 1999, CALSTIS Reference Guide (Greenbelt: NASA/LASP)
Linsky, J. L., Valenti, J., & Johns-Krull, C. M. 1999, BAAS, 195, 214
McMurry, A. D., & Jordan, C. 2000, MNRAS, 313, 423
Muzerolle, J., Calvet, N., Briceno, C., Hartmann, L., & Hillenbrand, L. 2000, ApJ, 535, L47
Muzerolle, J., Calvet, N., & Hartmann, L. 2001, ApJ, 550, 944
Najita, J., Carr, J. S., Glassgold, A. E., Shu, F. H., & Tokunaga, A. T. 1996, ApJ, 462, 919
Reipurth, B., & Bally, J. 2001, ARA&A, 39, 403
Richter, M. J., Jaffe, D. T., Blake, G. A., & Lacy, J. H. 2001, BAAS, 199, 6005
Roberge, A., et al. 2001, ApJ, 551, L97
Rucinski, S. M., & Krautter, J. 1983, A&A, 121, 217
Sitko, M. L., Russell, R. W., & Lynch, D. K. 2000, AJ, 120, 2609

Strom, S. E., Edwards, S., & Skrutskie, M. F. 1993, in Protostars and Planets III, ed. E. H. Levy & J. I. Lunine (Tucson: Univ. Arizona Press), 837
Thi, W. F., et al. 2001, ApJ, 561, 1074
Torres, G., Stefanik, R. P., Latham, D. L., & Mazeh, T. 1995, ApJ, 452, 870
Trilling, D. E., Koerner, D. W., Barnes, J. W., Ftaclas, C., & Brown, R. H. 2001, ApJ, 552, L151
Valenti, J. A., Johns-Krull, C. M., & Linsky, J. L. 2000, ApJS, 129, 399
van Langevelde, H. J., van Dishoeck, E. F., van der Werf, P. P., & Blake, G. A. 1994, A&A, 287, L25
van Zadelhoff, H. J., van Dishoeck, E. F., Thi, W. F., & Blake, G. A. 2001, A&A, 377, 566
Webb, R. A., Zuckerman, B., Patience, J., White, R. J., Schwartz, M. J., McCarthy, C., & Platais, I. 1999, ApJ, 512, L63
Weinberger, A. J., Schneider, G., Becklin, E. E., Smith, B. A., & Hines, D. C. 1999, BAAS, 194, 6904
Weinberger, A. J., et al. 2002, ApJ, 566, 409
Weintraub, D. A., Kastner, J. H., & Bary, J. S. 2000, ApJ, 541, 767
Wichmann, R., Bastian, U., Krautter, J., Jankovics, I., & Rucinski, S. M. 1998, MNRAS, 301, L39
Williams, D. A., et al. 2000, in Molecular Hydrogen in Space, ed. F. Combes & G. Pineau de Forets (Cambridge: Cambridge Univ. Press), 99
Wilner, D. J., Ho, P. T. P., Kastner, J. H., & Rodriguez, L. F. 2000, ApJ, 534, L101
Wolk, S. J., & Walter, F. M. 1996, AJ, 111, 2066
Wood, B. E., Karovska, M., & Raymond, 2002, ApJ, in press
Wuchterl, G., Guillot, T., & Lissauer, J. J. 2000, in Protostars and Planets IV, ed. V. Mannings, A. P. Boss, & S. S. Russell (Tucson: Univ. Arizona Press), 1081
Zuckerman, B. 2001, ARA&A, 39, 549